The Astronomical Journal, 156:251 (14pp), 2018 December https://doi.org/10.3847/1538-3881/aae0f7

A Tale of "Two" Comets: The Primary Volatile Composition of Comet 2P/Encke Across Apparitions and Implications for Cometary Science

Nathan X. Roth[1,8], Erika L. Gibb[1,2,8], Boncho P. Bonev[2,3,8], Michael A. DiSanti[2,4,8], Neil Dello Russo[5,8], Ronald J. Vervack, Jr.[5,8], Adam J. McKay[4,6,8], and Hideyo Kawakita[7,8]

[1] Department of Physics & Astronomy, University of Missouri-St. Louis, One University Blvd., St. Louis, MO, USA; nxrq67@mail.umsl.edu
[2] Goddard Center for Astrobiology, NASA-Goddard Space Flight Center, Greenbelt, MD, USA
[3] Department of Physics, American University, Washington, DC, USA
[4] Solar System Exploration Division, Planetary System Laboratory Code 693, NASA-Goddard Space Flight Center, Greenbelt, MD, USA
[5] Johns Hopkins University Applied Physics Laboratory, Laurel, MD, USA
[6] Universities Space Research Association/NASA Postdoctoral Program, Columbia, MD, USA
[7] Koyama Astronomical Observatory, Kyoto Sangyo University Motoyama, Kamingamo, Kita-ku, Kyoto 603-8555, Japan
Received 2018 May 8; revised 2018 September 5; accepted 2018 September 10; published 2018 November 7

Abstract

The highly favorable 2017 apparition of 2P/Encke allowed the first comprehensive comparison of primary volatile abundances in a given comet across multiple apparitions. This apparition offered opportunities to address pressing questions in cometary science, including investigating evolutionary and/or heliocentric distance (R_h) effects on volatile production, sampling the hypervolatiles CO and CH_4 in an ecliptic comet, and measuring volatile release at small R_h. The faintness and frequently low geocentric velocity of ecliptic comets during most apparitions make our near-infrared observations of these hypervolatiles rare and of high scientific impact. We characterized the volatile composition of 2P/Encke on three post-perihelion dates using the iSHELL spectrograph at the NASA Infrared Telescope Facility on Maunakea, HI. We detected fluorescent emission from nine primary volatiles (H_2O, CO, C_2H_6, CH_3OH, CH_4, H_2CO, NH_3, OCS, and HCN) and three fragment species (OH^*, NH_2, and CN), and obtained a sensitive upper limit for C_2H_2. We report rotational temperatures, production rates, and mixing ratios (abundances relative to H_2O). Compared to mean abundances in comets observed to date in the near-infrared, mixing ratios of trace gases in 2P/Encke were depleted for all species except H_2CO and NH_3, which were "normal." The detection of the hypervolatiles CO and CH_4 is particularly notable given the paucity of measurements in ecliptic comets. We observed significant differences in primary volatile composition compared to published pre-perihelion results from 2003 at larger R_h. We discuss possible mechanisms for these differences and discuss these results in the context of findings from the *Rosetta* mission and ground-based studies of comets.

Key words: comets: general – comets: individual (2P/Encke) – techniques: spectroscopic

1. Introduction

Understanding the evolution of the solar system, as well as its current volatile content, requires knowledge of the initial conditions present in the solar nebula. As some of the first objects to accrete in the solar nebula, cometary nuclei are among the most primitive remnants of solar system formation. Lacking a mechanism for efficient internal self-heating owing to their small sizes, their initial volatile composition likely reflects the composition and conditions where (and when) they formed. However, for short-period comets, there is some question of how repeated passages through the inner solar system may affect volatile compositions. High-resolution near-infrared spectroscopy offers a unique and valuable tool for sampling the primary volatile (i.e., ices sublimating directly from the nucleus) composition of comets via analysis of fluorescent emission in cometary comae. To date, over 30 comets have been characterized in this manner. Combined with extensive work at optical and radio wavelengths, these results have shown that there is a high diversity of volatile compositions in the comet population. Unlike Oort cloud comets (OCCs), which can generally be observed only during a single apparition (exceptions are Halley-type comets with shorter orbital periods, such as 8P/Tuttle), short-period comets offer the opportunity to investigate potential evolutionary effects on volatile composition.

The majority of comets that become available for remote sensing can be placed into one of two dynamical groups: (1) Ecliptic comets, such as the Jupiter-family comets (JFCs) and 2P/Encke (the subject of our study), which originate principally from the scattered Kuiper disk and have small orbital inclinations, and (2) nearly isotropic OCCs, which originate from the outer reaches of the solar system and have random orbital inclinations. Historically, OCCs were thought to form in situ at heliocentric distances (R_h) between 5 and 30 au before being scattered to the Oort cloud, whereas ecliptic comets formed separately at even larger heliocentric distances. However, the detections of crystalline silicates in comets 1P/Halley (Bregman et al. 1987), C/1995 O1 (Hale-Bopp) (*ISO*; Crovisier et al. 1996), C/2001 Q4 (NEAT) (HIFOGS; Wooden et al. 2004), 9P/Tempel 1 (via remote observations of material ejected during the Deep Impact mission; Harker et al. 2005), and 81P/Wild 2 (in grains returned by the Stardust mission; Zolensky et al. 2006) imply that material in their nuclei was processed at small R_h and mixed over ranges of distances in the solar nebula. Coupled with more recent dynamical modeling (e.g., Gomes et al. 2005; Morbidelli et al. 2005; Levison et al. 2011), this evidence suggests that comet formation was instead a more "spatially mixed" process.

[8] Visiting Astronomer at the Infrared Telescope Facility, which is operated by the University of Hawaii under contract NNH14CK55B with the National Aeronautics and Space Administration.

Given this complex scenario, the volatile compositions of cometary nuclei may represent widely varying (or at the other extreme, largely overlapping) formation regions in the solar nebula. Heterogeneous nuclei, such as 67P/Churyumov–Gerasimenko (Rickman et al. 2015), introduce another layer of complexity in tying the compositions of cometary nuclei to a particular formation history or region in the solar nebula. Additionally, evolutionary effects over the ~4.5 billion year lifetime of comets must be considered. Although most processes considered to alter the properties of the nucleus are expected to affect a thin (at most a few meters deep) layer near the surface over the course of a typical perihelion passage (see Stern 2003 for a discussion of these processes for OCCs), an ecliptic comet experiencing many perihelion passages, particularly at small R_h, may suffer considerable processing compared to a dynamically new OCC entering the inner solar system for the first time. Indeed, measured JFCs are on average depleted in their primary volatiles relative to OCCs (Dello Russo et al. 2016a). Understanding potential evolutionary effects, including systematic differences between ecliptic comets and OCCs, is critical to interpreting the clues of solar system formation that are imprinted in the ices of cometary nuclei, as well as to placing the results of present-day observations into a meaningful context.

Interpreting the results of volatile composition studies requires overcoming observational biases. Thus far, near-infrared studies of primary volatile composition have largely been "snapshots"—observations over a single apparition and at most a small range of R_h (often near ~1 au) for comets that, in many cases, will make a single perihelion passage during a human lifetime. Although several comets have been observed in the near-infrared at small R_h (<0.8 au, e.g., DiSanti et al. 2003, 2016, 2017; Gibb et al. 2003) and large R_h (>2 au, e.g., Magee-Sauer et al. 1999; Brooke et al. 2003; Paganini et al. 2012; Kawakita et al. 2014; Bonev et al. 2017), to date no comets have had a complete primary volatile inventory characterized over multiple apparitions.

Additionally, certain primary volatiles (specifically, C_2H_2, OCS, CO, and CH_4) are underrepresented in studies of comets as a whole, and in particular in studies of ecliptic comets. In the case of C_2H_2 and OCS, this has been due largely to limitations in sensitivity and lack of spectral coverage, respectively. For CH_4 and CO, which as "hypervolatiles" can provide unique insights into the processing in the early solar system (Dello Russo et al. 2016a), their (highly opaque) telluric counterparts require sufficiently large geocentric velocity (Δ_{dot}) to Doppler-shift corresponding cometary emissions to regions of adequate atmospheric transmittance. To compensate for their low brightness, most observations of ecliptic comets take place near closest passage to Earth, coinciding with small Δ_{dot}, and so precluding measurement of CO and CH_4. This has resulted in a significant paucity of detections of CO and CH_4 in ecliptic comets at near-infrared wavelengths. Being a symmetric hydrocarbon, CH_4 can only be sampled in the near-infrared due to its lacking a dipole moment; however, CO is easily detectable at radio wavelengths and has been measured in several ecliptic comets (e.g., Crovisier et al. 2009).

Fortunately, the first quarter of 2017 provided the opportunity to address many of these pressing matters in cometary science with a highly favorable apparition of the unique ecliptic comet 2P/Encke (hereafter Encke). Encke is known for its weak dust production, asymmetric coma, and one of the shortest orbital periods among known comets (3.3 years). In terms of its dynamical history, Encke is truly unique among comets. In addition to its small perihelion distance ($q \sim 0.3$ au), Encke has the smallest known aphelion distance of any comet (4.1 au), distinguishing it from JFCs for which this is beyond Jupiter's orbit (5.2 au). Explaining how Encke evolved to its current orbit, along with the fact that it is still an active comet, has proven challenging. Increasingly sophisticated dynamical modeling efforts (Levison et al. 2006) suggest that after becoming decoupled from Jupiter, Encke accumulated a dust mantle and became temporarily inactive. Encke then evolved into the ν_6 secular resonance, causing its perihelion distance to slowly decrease, eventually blowing away its dust mantle, reigniting cometary activity, and dooming Encke to a collision with the Sun in 10^5–10^6 years.

We used the newly commissioned iSHELL spectrograph at the NASA Infrared Telescope Facility (IRTF) to characterize the volatile composition of Encke at small R_h (~0.4 au) and at high Δ_{dot} (~+27 km s^{-1}) on three post-perihelion dates. The excellent sensitivity, large spectral grasp, and daytime observing capabilities of iSHELL allowed us to securely measure CO and CH_4, to detect and stringently constrain OCS and C_2H_2, respectively, and to provide the first comprehensive characterization of primary volatile composition in a comet across multiple perihelion passages by comparing to published results from the 2003 apparition (Radeva et al. 2013—hereafter referred to as RD13). In Section 2, we discuss our observations and data analysis. In Section 3, we present our results. In Section 4, we compare our results to those of RD13 and discuss possible mechanisms for observed differences in volatile composition. In Section 5, we discuss Encke's place in the context of other comets characterized to date.

2. Observations and Data Reduction

During its 2017 apparition, Encke reached perihelion on March 10 and was closest to Earth (0.65 au) on March 12. On UT 2017 March 21, 22, and 25, we observed Encke with the high-resolution ($\lambda/\Delta\lambda \sim 40000$), near-infrared, immersion-grating echelle spectrograph iSHELL (Rayner et al. 2012, 2016) at the 3 m NASA IRTF to characterize its volatile composition. We emphasize the unique ability of iSHELL to acquire spectral data at M-band during daytime while actively guiding on L-band emission (in this case, using a narrow-band 3.46 μm filter). This allowed us to achieve an observing efficiency of ~72% for our M-band observations of Encke.

We chose iSHELL settings (L1, Lp1, and M2) so as to fully sample a suite of molecular abundances. User-defined cross-disperser positions (specifically, L-Custom) first became available on our third and final date (March 25), which greatly facilitated simultaneous measurement of H_2O together with minor species (HCN, C_2H_2, NH_3, and NH_2) in the 3 μm region.

Observations were performed with a 6-pixel (0.″75) wide slit, using a standard ABBA nod pattern, with A and B beams symmetrically placed about the midpoint along the 15″ long slit and separated by half its length. Combining spectra of the nodded beams as A–B–B+A cancelled emissions from thermal background, instrumental biases, and "sky" emission (lines and continuum) to second order in air mass. The data were dark-subtracted, flat-fielded, and cleaned of cosmic ray hits and "hot" (high dark current) pixels. Flux calibration was performed using appropriately placed bright IR flux standard

Table 1
Observing Log and H_2O Production Rates in 2P/Encke

UT Date (2017)	iSHELL Setting	UT	R_h (au)	dR_h/dt (km s^{-1})	Δ (au)	$d\Delta/dt$ (km s^{-1})	T_{int} (minutes)	$Q(H_2O)$ (10^{28} s^{-1})
March 21	Lp1	19:52–20:54	0.456	29.05	0.751	26.84	34	3.53 ± 0.31
	L1	21:53–22:28	0.458	29.12	0.753	27.10	26	3.51 ± 0.11
March 22	M2	18:52–20:01	0.473	29.81	0.767	27.15	50	4.14 ± 0.16
March 25	L-Custom	17:49–20:43, 21:53–22:22	0.526	31.34	0.814	27.18	96	2.89 ± 0.06

Note. R_h, dR_h/dt, Δ, and $d\Delta/dt$ are heliocentric distance, heliocentric velocity, geocentric distance, and geocentric velocity, respectively, of 2P/Encke; T_{int} is total integration time on source, and $Q(H_2O)$ is the global water production rate described in Section 2. Seeing increased over the course of the day from ∼0.″6 to ∼1.″2, from 0.″6 to ∼2″, and from ∼1″ to 1.″5 on March 21, 22, and 25, respectively. The column burden of atmospheric water vapor (expressed in precipitable millimeters) retrieved in fitting synthetic telluric absorption models to flux standard star continua was 1.7, 1.2, and 1.8 on March 21, 22, and 25, respectively.

stars on each date using a wide (4.″0) slit. The observing log is shown in Table 1.

Our well-established data reduction procedures are described extensively in the refereed literature (Bonev 2005; DiSanti et al. 2006, 2014; Villanueva et al. 2009; Radeva et al. 2010). Their application to unique aspects of iSHELL spectra is detailed in Section 3.2 of DiSanti et al. (2017). We determined contributions from continuum and gaseous emissions in our comet spectra as previously described (e.g., DiSanti et al. 2016), and illustrate the procedure in Figure 1. We convolved the fully resolved transmittance function to the resolving power of the data (∼4.0 × 10^4) and scaled it to the level of the comet continuum. We then subtracted the modeled continuum to isolate cometary emission lines. Synthetic models of fluorescent emission for each targeted species were compared to observed line intensities, after correcting each modeled line intensity for the monochromatic atmospheric transmittance at its Doppler-shifted wavelength (according to the geocentric velocity of the comet at the time of the observations).

Nucleocentric (or "nucleus-centered") production rates (Q_{NC}) were determined using our well-documented formalism (Dello Russo et al. 1998; DiSanti et al. 2001; Bonev 2005; Villanueva et al. 2011); see Section 3.2.2 of DiSanti et al. (2016) for further details. The nucleocentric production rates were multiplied by an appropriate growth factor (GF), which was determined using our Q-curve methodology (e.g., DiSanti et al. 2001; Bonev 2005; Gibb et al. 2012) that relates molecular production rates in the fraction of the coma along the column described by the beam (of size 0.″75 × 2.″5) to a "global" production rate, Q_{global}. Global production rates for all detected molecules are listed in Table 2. GFs were determined for both the gas and the dust when the signal-to-noise ratio (S/N) was sufficiently high (i.e., only for water and OH prompt emission, henceforth denoted OH*). Because OH* is well established as a reliable proxy for the production and spatial distribution of its parent, H_2O (Mumma et al. 2001; Bonev et al. 2006; Bonev & Mumma 2006), these two species provided similar GFs (see Table 2).

We note that the Q-curve methodology assumes a spherically symmetric coma and constant gas outflow speed. Although this spherically symmetric approach does not reproduce the aspherical and asymmetric coma of Encke (see Ihalawela et al. 2011; Dorman et al. 2013, and refs. therein), the calculated abundances (relative to water) should be accurate, since it was established that "symmetrizing" Q_{global} by averaging values to either side of the nucleus provides a reliable measure of total molecular production

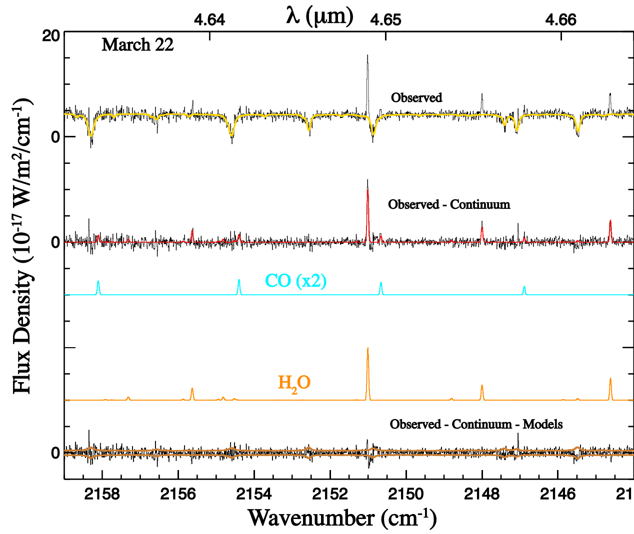

Figure 1. Extracted spectra showing clear detections of CO and H_2O in comet Encke superimposed on the cometary continuum on UT 2017 March 22. The gold trace overplotted on the uppermost cometary spectrum is the telluric absorption model (convolved to the instrumental resolution). Directly below is the residual spectrum (after subtracting the telluric absorption model), with the total modeled fluorescent emission overplotted in red. Individual fluorescent emission models (color-coded by species) are plotted below, offset vertically for clarity. At the bottom of the panel is the residual spectrum (after subtracting the telluric absorption model and all relevant molecular fluorescent models), with the 1σ uncertainty envelope overplotted in bronze.

rate (Xie & Mumma 1996a, 1996b). Furthermore, any over (or under) estimate in volatile production rates introduced by the model will apply to all volatiles with similar spatial distributions and cancel out in determining relative abundances.

3. Results

3.1. Spatial Profiles

We were able to extract spatial profiles of emission for H_2O, OH* (prompt emission), CO, and CH_3OH in Encke. Figure 2(A) shows spatial profiles of co-measured emissions in Encke for OH*, CH_3OH, and dust on March 21. Figure 2(B) shows the same for H_2O, CO, and dust on March 22. The CO and CH_3OH profiles were smoothed by 3 pixels due to low S/N. Emissions from dust on both dates show Encke's peculiar sunward-facing fan, which has been consistently observed during its perihelion passages for over a century (Sekanina 1988a, 1988b). While low S/N prevents definitive conclusions, Figure 2(A) suggests that the CH_3OH emission may have

Table 2
Volatile Composition of Comet 2P/Encke

iSHELL Setting	Molecule	T_{rot}[a] (K)	Growth Factor[b]	Q[c] (10^{25} mol s^{-1})	Q_x/Q_{H2O}[d] (%)
2017 Mar 21, $R_h = 0.456$ au, $\Delta = 0.751$ au, $d\Delta/dt = 27.0$ km s^{-1}					
L1	H_2O	68^{+2}_{-3}	2.04 ± 0.23	3505 ± 111	100
	HCN	78^{+15}_{-12}	(2.04)	6.20 ± 0.50	0.18 ± 0.02
		(68)	(2.04)	5.89 ± 0.47	0.17 ± 0.02
Lp1	C_2H_6	(68)	(1.82)	1.29 ± 0.14	0.037 ± 0.005
	CH_3OH	52^{+7}_{-6}	(1.82)	27.5 ± 1.5	0.78 ± 0.08
		(68)	(1.82)	30.7 ± 1.8	0.87 ± 0.09
	CH_4	(68)	(1.82)	3.74 ± 0.28	0.11 ± 0.01
	H_2CO	(68)	(1.82)	9.42 ± 1.05	0.27 ± 0.04
	OH^*	(68)	1.82 ± 0.19	3534 ± 313	100
2017 Mar 22, $R_h = 0.473$ au, $\Delta = 0.767$ au, $d\Delta/dt = 27.1$ km s^{-1}					
M2	H_2O	67 ± 6	2.25 ± 0.11	4141 ± 158	100
	CO	(67)	(2.25)	17.9 ± 1.5	0.43 ± 0.04
	OCS	(67)	(2.25)	2.65 ± 0.55	0.06 ± 0.01
2017 Mar 25, $R_h = 0.526$ au, $\Delta = 0.814$ au, $d\Delta/dt = 27.2$ km s^{-1}					
L-Custom (2.9–3.1 μm)	H_2O	63 ± 2	2.02 ± 0.20	2890 ± 62	100
	HCN	66^{+16}_{-11}	(2.02)	3.23 ± 0.26	0.11 ± 0.01
		(63)	(2.02)	3.20 ± 0.25	0.11 ± 0.01
	C_2H_2	(63)	(2.02)	<0.2 (3σ)	<0.007 (3σ)
	NH_3	(63)	(2.02)	17.8 ± 1.1	0.61 ± 0.04
	NH_2	(63)	(2.02)	6.81 ± 1.01	0.23 ± 0.03

Notes.
[a] Rotational temperature. Values in parentheses are assumed.
[b] Growth factor. Values in parentheses are assumed.
[c] Global production rate. Uncertainties in production rate include line-by-line deviation between modeled and observed intensities and photon noise (see Dello Russo et al. 2004; Bonev 2005; Bonev et al. 2007).
[d] Molecular abundance with respect to H_2O.

peaked sunward of the OH^* emission on March 21, and Figure 2(B) suggests that the CO emission may have been narrower than that for the dust, while the H_2O emission was broader.

3.2. Mixing Ratios of Volatile Species

3.2.1. Molecular Fluorescence Analysis

Synthetic models of fluorescent emission for each targeted species were compared to observed line intensities, after correcting each modeled line intensity (g-factor) for the monochromatic atmospheric transmittance at its Doppler-shifted wavelength (according to the geocentric velocity of the comet at the time of the observations). The g-factors used in synthetic fluorescent emission models in this study were generated with quantum mechanical models developed for each molecule, with original publications cited in Section 3.2 of Paganini et al. (2014). A Levenberg–Marquardt nonlinear minimization technique (Villanueva et al. 2008) was used to fit fluorescent emission from all species simultaneously in each echelle order, allowing for high-precision results, even in spectrally crowded regions containing many spectral lines within a single instrumental resolution element. Production rates for each sampled species were determined from the appropriate fluorescence model at the rotational temperature of each molecule (Section 3.2.2).

3.2.2. Determination of Rotational Temperature

Rotational temperatures were determined using correlation and excitation analyses as described in Bonev (2005, pp. 53–65), Bonev et al. (2008), DiSanti et al. (2006), and Villanueva et al. (2008). In general, well-constrained rotational temperatures can be determined for individual species having intrinsically bright lines and for which a broad range of excitation energies is sampled. Utilizing the large spectral grasp of iSHELL, in the case of H_2O we were able to sample dozens of strong lines simultaneously.

We performed a fluorescence analysis for multiple molecules on all dates (including H_2O) and found consistent rotational temperatures. The rotational temperature (T_{rot}) for H_2O was well-constrained and was consistent (within 1σ uncertainty) on all dates (being 62^{+2}_{-3} K, 67 ± 6 K, and 63 ± 2 K on March 21, 22, and 25, respectively). Rotational temperatures retrieved for other molecules are listed in Table 2. When a rotational temperature for a particular molecule could not be retrieved, we assumed the rotational temperature from simultaneously measured H_2O within the same setting. In general, rotational temperatures agree for different primary species measured at infrared wavelengths (see for example Gibb et al. 2012 and references therein; also see Section 3.2.1 of DiSanti et al. 2016), supporting this approach.

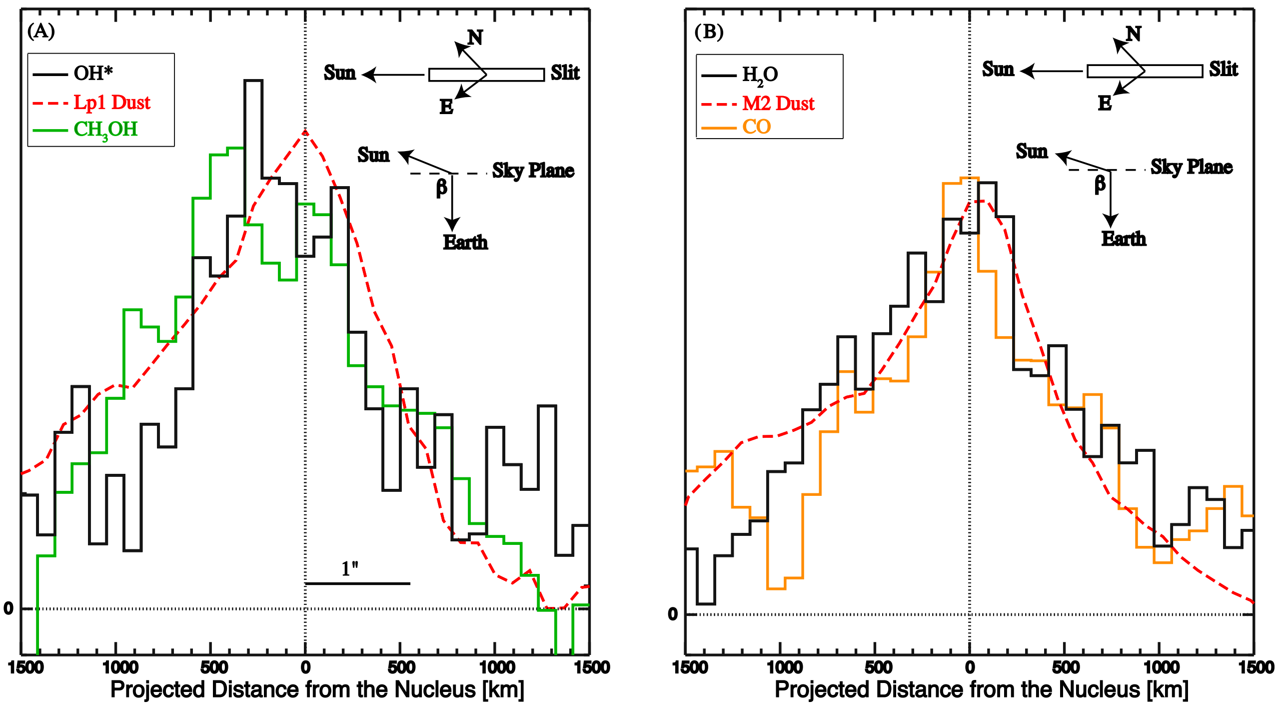

Figure 2. (A) Spatial profiles of co-measured emissions in Encke for OH* (prompt emission, black), CH_3OH (green) and dust (red) on UT 2017 March 21. The slit was oriented along the projected Sun-comet line (position angle 234°), with the Sun-facing direction to the left as indicated. Also shown is the Sun-comet-Earth angle (phase angle, β) of 108°, so largely in the sky plane. The horizontal bar indicating $1''$ corresponds to a projected distance of approximately 550 km at the geocentric distance of Encke. (B) Spatial profiles of co-measured emissions for H_2O (black), CO (orange), and dust (red) on UT 2017 March 22. The CO and CH_3OH profiles have been smoothed by 3 pixels. The observing geometry on March 22 was similar to that of March 21, with a position angle of 234° and a phase angle of 104°.

3.2.3. Secure Detections of CO and CH_4

Our detections of the hypervolatiles CO and CH_4 in Encke are particularly notable for two reasons: (1) The paucity of measurements of CO and CH_4 in ecliptic comets in general, and (2) the measurement of these hypervolatiles in the most thermally evolved comet known. Of all primary volatiles systematically measured in comets, these two molecules are most sensitive to thermal processing, but as noted earlier, they are also among the most difficult to sample from the ground due to lack of sensitivity and/or adequate geocentric velocity. Encke's excellent geocentric velocity ($>+27\ \mathrm{km\ s^{-1}}$ for all dates) allowed us to secure firm detections of both species. Each hypervolatile has been detected in less than 10 ecliptic comets (most below the 5σ level), making our measurements in Encke a critical component in establishing statistics for these species in ecliptic comets, and determining the importance of natal versus evolutionary effects on present comet volatile composition. Figures 1 and 3(A) show clear CO, H_2O, and CN emissions in Encke superimposed on the cometary continuum, and Figures 3(B)–(C) show corresponding detections for CH_4, C_2H_6, and CH_3OH, along with (co-measured) OH*.

3.2.4. Other Volatiles

In the 3 μm region, we securely detected emission from the nitrogen-bearing species HCN (Figure 4(A)), as well as NH_3 (Figure 4(B)) for the first time in Encke. We stringently constrained C_2H_2 (Figure 4(A)), obtaining a (3σ) upper limit (<0.007% relative to H_2O; Table 2) that is consistent with (but well below) that reported by RD13 (<0.08%–0.10%). Figure 4(C) shows Order 179, which samples H_2O lines spanning a broad range of rotational energies and thus is particularly diagnostic of T_{rot}. We also detected OCS with signal-to-noise exceeding 4σ (Figure 4(E)), representing its first reported abundance in Encke. CN emissions in Encke were strong (Figure 4(E)) consistent with that seen in other comets measured at small R_h (e.g., Dello Russo et al. 2016a). We defer a more detailed analysis of CN to a future publication.

In the Lp1 setting, we simultaneously detected (in Orders 154 and 155) C_2H_6 ν_7 band emission together with CH_3OH ν_2 band and CH_4 ν_3 P-branch lines (Figure 3(C)). We also co-measured CH_3OH ν_3 band, H_2CO ν_5 band, H_2CO ν_1 band (Figure 4(D)), and CH_4 ν_3 R-branch lines (Figure 3(B)). These were sampled simultaneously with OH* in five orders. We used the value of $Q(H_2O)$ so determined in establishing mixing ratios (i.e., abundances relative to H_2O) for C_2H_6, CH_3OH, CH_4, and H_2CO.

4. Comparisons with 2003 and Other Comets Measured

The 2017 apparition of Encke provided an opportunity to conduct the first comprehensive comparison of primary volatile composition through multiple perihelion passages, thereby allowing us to address pressing questions in cometary science. These include testing possible evolutionary and/or heliocentric distance effects on volatile production, and also examining asymmetries in volatile production about perihelion. We discuss each of these topics in turn, and place Encke in the context of other comets observed to date.

4.1. Dramatic Compositional Differences Compared to the 2003 Apparition

We observed dramatic differences in the primary volatile composition of Encke compared to the 2003 apparition. RD13 characterized the primary volatile composition of Encke in 2003 at $R_h \sim 1.2$ au pre-perihelion using NIRSPEC at the

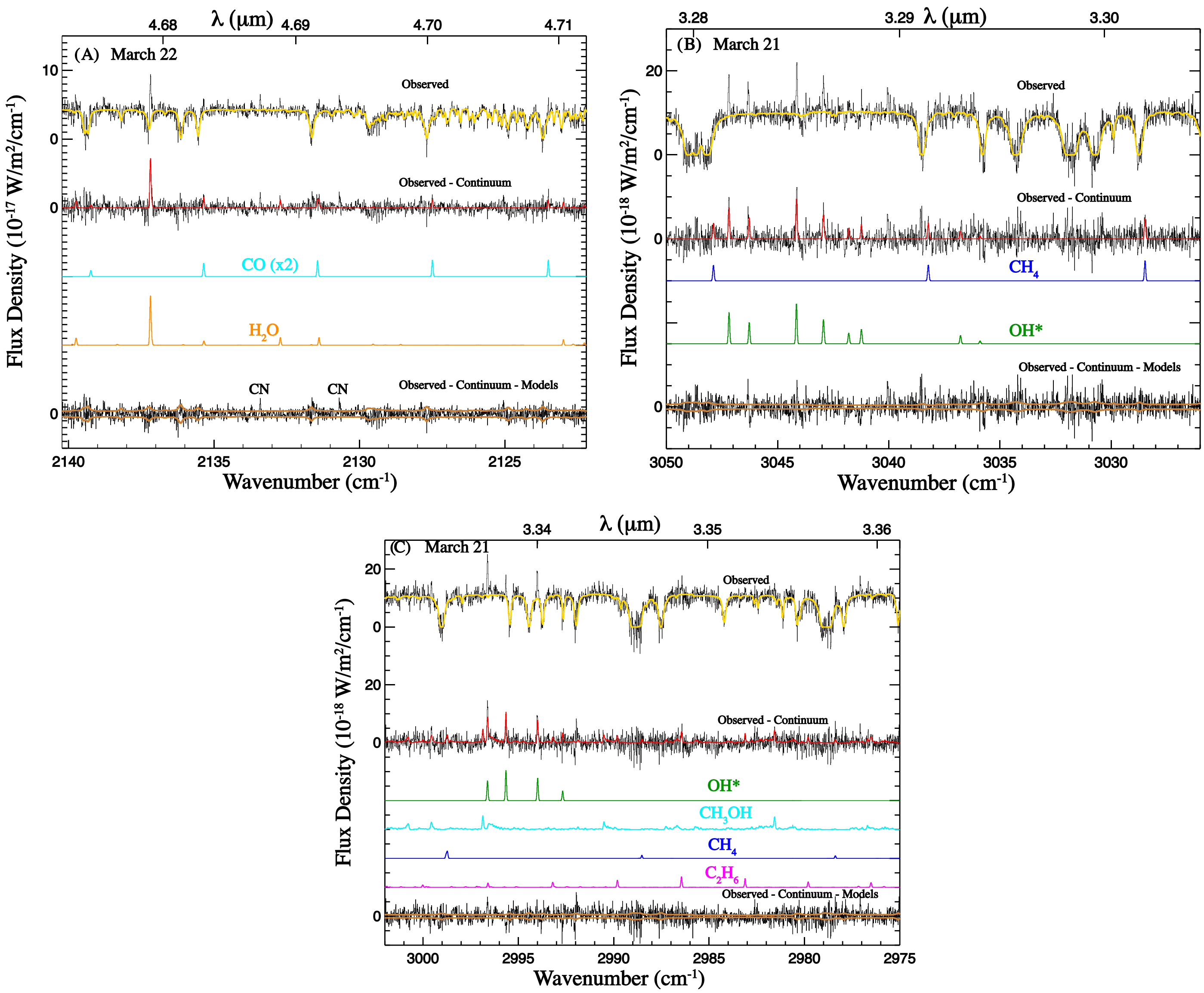

Figure 3. (A) Extracted spectra showing detections of CO, H_2O, and CN in comet Encke on UT 2017 March 22, with traces and labels as described in Figure 1. (B)–(C) Detections of CH_4, C_2H_6, CH_3OH, and OH* (prompt emission) on UT 2017 March 21.

W.M. Keck Observatory. Table 3 shows a comparison of results from 2003 and 2017. Figure 5 provides the same comparison graphically, along with near-infrared measurements of each volatile in comets to date and their respective mean values among comets (Dello Russo et al. 2016a; DiSanti et al. 2017). The contrast between the two apparitions is obvious. Figure 5 illustrates that:

1. CH_3OH (0.87%), C_2H_6 (0.037%), and CH_4 (0.11%) show clear depletion, both with respect to the 2003 apparition as well as among measured comets. The 2003 measurement of CH_3OH (3.48%) placed Encke among the most CH_3OH-enriched comets observed to date, whereas the 2017 measurement is clearly depleted. Similarly, the C_2H_6 mixing ratio (depleted by a factor of 10 compared to 2003) is the lowest measured in any comet to date.
2. H_2CO (0.27%) and HCN (0.12%) are enriched compared to their respective 2003 abundances. H_2CO is strongly enriched (by greater than a factor of 2) and consistent with the mean value among comets, and HCN is moderately enriched (by less than a factor of 2) from 2003 but is slightly less than its mean value.
3. NH_3 was not reported in RD13, but its value in 2017 (0.61%) is consistent with its mean. The mixing ratio for CO (0.43%) and the (3σ) upper limit for C_2H_2 (<0.007%) are both consistent with upper limits reported for 2003, and both are strongly depleted compared to their respective mean values.

4.2. Interpreting Differences in the Volatile Content of Encke Across Apparitions

The most striking feature of the primary volatile composition of Encke during the 2017 apparition is its difference from that reported for 2003. Understanding the cause(s) of these differences—and their significance—is crucial to tying observed primary volatile compositions to formative conditions in the solar nebula. We examine (in turn) four possible explanations for these differences, each of which may have

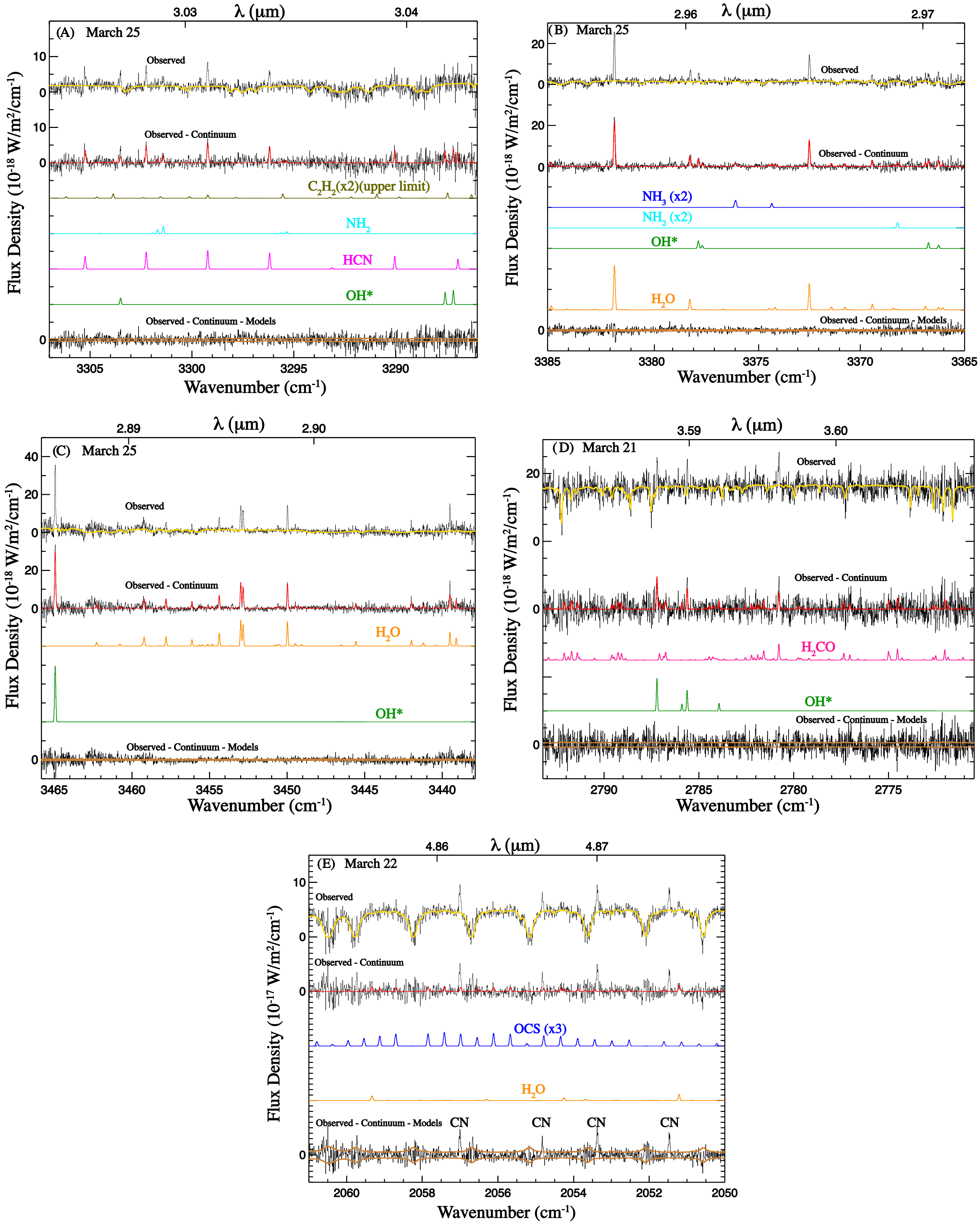

Figure 4. (A)–(C) Extracted spectra showing detections of HCN, NH_2, NH_3, H_2O, and OH^* (prompt emission), as well as determination of T_{rot} for H_2O, on UT 2017 March 25. (D) Detections of H_2CO and OH^* on UT 2017 March 21. (E) Detections of OCS, H_2O, and CN on UT 2017 March 22.

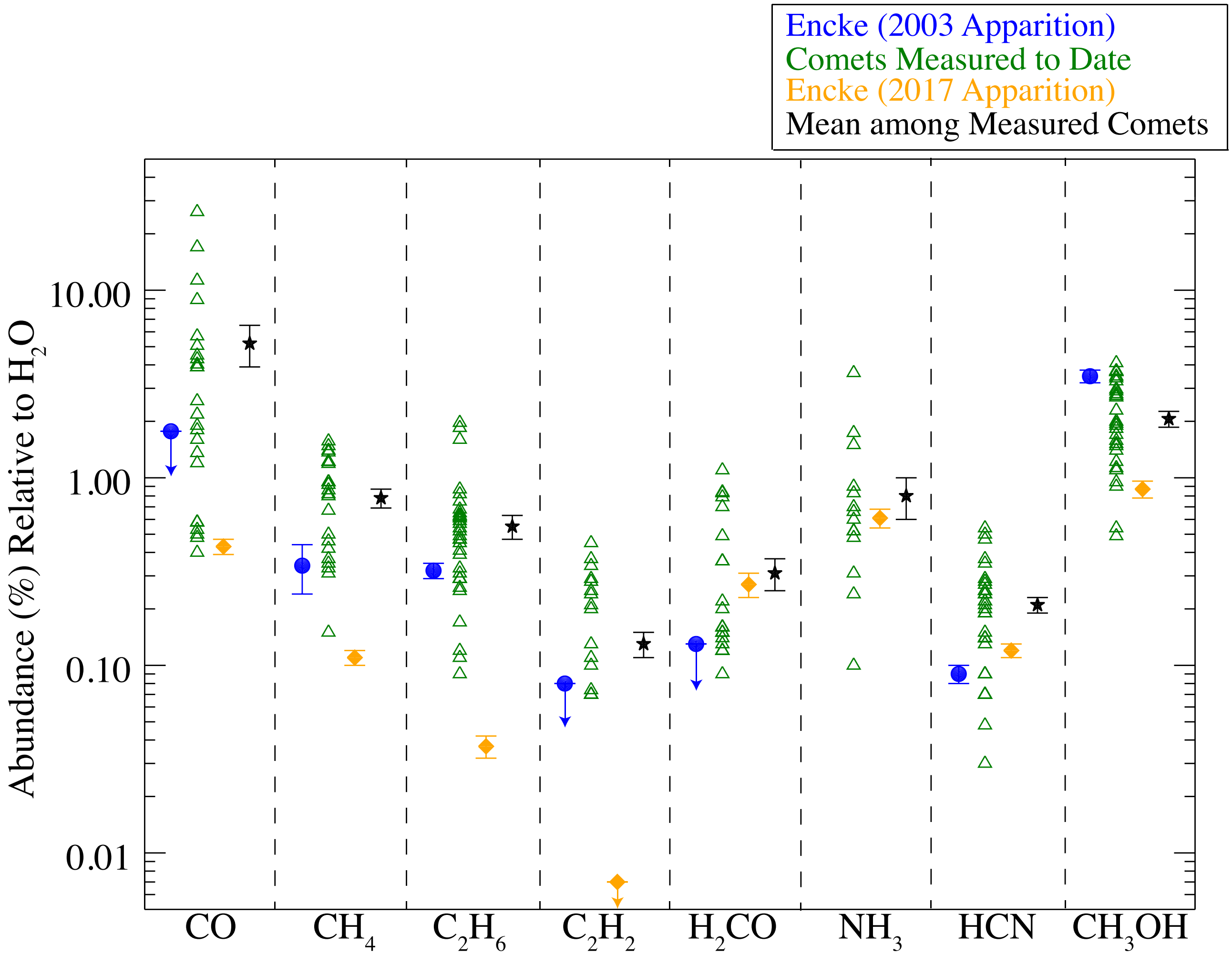

Figure 5. Comparison of mixing ratios (%, relative to H_2O) of primary volatiles sampled in Encke during the 2003 (blue, Radeva et al. 2013) and 2017 (orange, this work) perihelion passages, as well as near-infrared measurements of each volatile in comets to date (green) and their respective mean values (black, Dello Russo et al. 2016a; DiSanti et al. 2017). Error bars indicate measurements, whereas downward arrows indicate 3σ upper limits.

contributed simultaneously and to varying degrees: (1) dependence on heliocentric distance, (2) evolutionary processing of a heterogeneous nucleus, (3) pre-/post-perihelion asymmetries in volatile mixing ratios, and (4) viewing geometry effects.

4.2.1. Dependence of Volatile Production on Heliocentric Distance

As noted earlier, near-infrared spectroscopic studies of comets spanning large ranges of heliocentric distances during a given apparition are sparse. Provided that the primary volatile composition of the coma accurately reflects the composition of ices in the nucleus once sublimation of all volatiles has been completely activated, then mixing ratios of primary volatiles in comet comae should remain relatively constant once H_2O controls the overall activity (assuming compositional homogeneity). Comets observed to date in the near-infrared suggest that this is true in general, although some primary volatiles (NH_3, H_2CO, and C_2H_2) and fragment species (CN and NH_2) show enhanced production at $R_h < 0.8$ au (possibly due to release from grains; e.g., see Dello Russo et al. 2016a). Measurements at radio wavelengths have also shown that H_2CO may originate from extended sources (e.g., Cordiner et al. 2014) and clearly shows increasing abundances with

Table 3
Primary Volatile Abundances in 2P/Encke Across Apparitions

Molecule	2017 Apparition[a] %, Relative to H_2O	2003 Apparition[b] %, Relative to H_2O	Mean Value among Comets[c]
C_2H_6	0.037 ± 0.005	0.32 ± 0.03	0.55 ± 0.08
CH_3OH	0.87 ± 0.09	3.48 ± 0.27	2.06 ± 0.20
CH_4	0.11 ± 0.01	0.34 ± 0.10	0.78 ± 0.09
CO	0.43 ± 0.04	<1.77	5.2 ± 1.3
HCN	0.12 ± 0.01	0.09 ± 0.01	0.21 ± 0.02
NH_3	0.61 ± 0.04	…	0.80 ± 0.20
H_2CO	0.27 ± 0.04	<0.13	0.31 ± 0.06
C_2H_2	<0.007	<0.08	0.13 ± 0.02
OCS	0.06 ± 0.01	…	…

Notes.
[a] This work. Abundances are given as weighted averages for molecules detected on multiple dates. Upper limits for non-detected species are 3σ. In all cases values are expressed relative to simultaneously measured H_2O.
[b] Abundances taken from Radeva et al. (2013).
[c] Mean values and 1σ uncertainties among measured comets taken from Dello Russo et al. (2016a). No value is listed for OCS due to the paucity of measurements at near-infrared wavelengths.

decreasing R_h, possibly due to thermal degradation of polymers (Fray et al. 2006). Although we were not able to extract spatial profiles of H_2CO emission with adequate S/N to test for the presence of an extended source, the enrichment of H_2CO in 2017 (0.27%, $R_h \sim 0.4$ au) compared to 2003 (<0.13%, $R_h \sim 1.2$ au) suggests this may be the case in Encke.

DiSanti et al. (2016) found that HCN became enriched in comet D/2012 S1 (ISON) at small R_h relative to measurements at larger R_h, increasing from 0.07% at $R_h = 0.82$ au to 0.26% at $R_h = 0.43$ au. We observed a similar trend in HCN with Encke in 2017 (0.17%, $R_h = 0.45$ au on March 21) compared to 2003 (0.09%, $R_h \sim 1.2$ au). However, HCN in Encke decreased from 0.17% to 0.11% on March 25 at $R_h = 0.53$ au. Given the nearly four-fold increase in HCN in ISON between $R_h = 0.83$ and 0.46 au, it is possible that the decrease in HCN in Encke from March 21 to March 25 may also be explained by its receding 0.08 au from the Sun. However, this does not explain the severe depletions of CH_3OH, C_2H_6, and CH_4 in 2017 compared to 2003, leaving the question unresolved. Clearly, further serial measurements of Encke over a range of R_h are needed to distinguish the possible dependence of its volatile composition on heliocentric distance from other factors.

4.2.2. Potential Evolutionary Processing of a Heterogeneous Nucleus

Our near-infrared measurements do not resolve the nucleus, and the few comets for which the structure of the nucleus is known are those visited by spacecraft. The *Rosetta* mission found a heterogeneous nucleus for comet 67P/Churyumov–Gerasimenko that is likely a contact binary (Rickman et al. 2015). In Encke, it is possible we are viewing compositional differences within a heterogeneous nucleus. This suggests two possibilities—(1) a compositionally different area dominated its activity in 2017 compared to 2003 (seasonal differences), or (2) subsequent perihelion passages have exhausted material that was active during 2003, and new material within the nucleus that was covered during the 2003 apparition was exposed in 2017 (evolutionary changes). In light of our measurements of compositional diversity from 2003 to 2017, it is noteworthy that pre-perihelion optical observations of Encke from McDonald Observatory during 2003 and 2017 show no remarkable changes in composition (A. McKay 2018, personal communication). This suggests that seasonal effects may dominate evolutionary changes in the bulk composition of Encke.

4.2.3. Asymmetry in Volatile Mixing Ratios About Perihelion Due to Seasonal Effects

Another possible explanation for the observed differences in Encke's composition is asymmetry in volatile mixing ratios about perihelion, in which distinct, chemically heterogeneous sources on the nucleus dominate volatile release due to seasonal effects. We were granted observing time to investigate such asymmetries in Encke with iSHELL; however, unfortunately our pre-perihelion run was completely weathered out.

Asymmetry in mixing ratios of fragment species about perihelion has been reported in the literature for Encke. A'Hearn et al. (1985) found that OH (and by proxy, water) production was symmetric about perihelion, whereas C_2, C_3, and CN production was much lower post-perihelion versus pre-perihelion. If this asymmetry in fragment species production has persisted to the present day, then we might expect that our post-perihelion observations (obtained <20 days post-perihelion) should show depletion in potential parent species for these fragments compared to the observations reported in RD13 (obtained >30 days pre-perihelion). Although direct comparisons between mixing ratios of primary volatile and fragment species are difficult owing to the complicated lineage of fragment species (e.g., multiple molecules, dust grain sources), our results support this hypothesis, with the important exceptions of HCN and H_2CO. As noted earlier, our abundance ratios HCN/H_2O and H_2CO/H_2O are enriched compared to that reported in RD13, perhaps due to additional sources becoming active at the small heliocentric distances of our observations.

Nonuniform volatile mixing ratios have been observed in other comets, perhaps most notably during the *Rosetta* mission to comet 67P/Churyumov–Gerasimenko. At comet 67P/C-G, *Rosetta* found that mixing ratios of CO and CO_2 in the coma varied due to seasonal effects on the nucleus (Hässig et al. 2015). Furthermore, variation in volatile mixing ratios was found on smaller timescales, with some volatiles (such as CH_4) showing diurnal variations that differed from those for other volatiles, such as CO and C_2H_6 (Luspay-Kuti et al. 2015; Bockelée-Morvan et al. 2016; Fink et al. 2016).

At comet 103P/Hartley 2, EPOXI/DIXI revealed a comet with distinct sources of outgassing on the nucleus. Strong CO_2 emission from the smaller lobe dragged icy grains along into the coma, from which ices sublimed and added to its gas content. In contrast, activity in the waist region was dominated by direct release of water gas (A'Hearn et al. 2011; Protopapa et al. 2014). Despite the heterogeneous outgassing at 103P/Hartley 2, ground-based observations showed that mixing ratios of trace species in the coma remained relatively constant (Dello Russo et al. 2011; Mumma et al. 2011).

Additionally, nonuniform mixing ratios of CO/H_2O were observed in comet C/2009 P1 (Garradd) by both ground-based studies (McKay et al. 2015) and space-based studies from the High Resolution Instrument Infrared Spectrometer aboard the *Deep Impact Flyby* spacecraft (Feaga et al. 2014). In C/2009 P1, H_2O production rates traced the predicted heliocentric dependence, rising and then falling near perihelion. However, CO production increased monotonically throughout the apparition, continuing to rise long after perihelion, perhaps due to seasonal effects on the nucleus (Bodewits et al. 2014; McKay et al. 2015).

Seasonal effects have been proposed to interpret imaging and photometric studies of Encke's coma (e.g., Sekanina 1988a; Ferrin 2008, and references therein; Farnham 2009), which suggest that (at least) two distinct nucleus sources receive seasonal illumination and account for outgassing in Encke during different portions of its orbit. However, there is debate regarding exactly when a given source activates and begins to dominate outgassing. Unfortunately, these observations are unable to trace the measured composition of the gases to individual source regions, and thus further test for compositional heterogeneity.

Perhaps the most compelling evidence linking the difference in primary volatile composition to the proposed existence of heterogeneous sources on the nucleus is the dramatic depletion of the least volatile trace species, CH_3OH, measured in Encke. RD13 reported $CH_3OH/H_2O = 3.48 \pm 0.27\%$ during the 2003 apparition, making Encke one of the most highly CH_3OH-enriched comets observed in the near-infrared. In contrast, our measured mixing ratio ($CH_3OH/H_2O = 0.87 \pm 0.09\%$) places Encke decisively among CH_3OH-depleted comets (see Figure 5 and Table 3). Combined with observed asymmetries in fragment species, the lack of bulk compositional changes seen at other wavelengths, and the observational evidence for seasonal effects governing outgassing in Encke, the "switch" from a highly CH_3OH-enriched comet to a CH_3OH-depleted comet (and other compositional differences observed in 2017 compared to 2003), may be explained by a combination of chemically heterogeneous nucleus sources and seasonal effects on Encke. That being said, contributions from additional sources activated at small R_h also cannot be ruled out, particularly since volatiles that have tended to show increased abundances or emission intensities in comets at small R_h (H_2CO, NH_3, NH_2, and CN) are generally enriched compared to other detected trace species in Encke in 2017.

4.2.4. Consideration of Viewing Geometry

Encke has displayed an aspherical and asymmetric coma in almost every recorded apparition since 1896 (Sekanina 1988a, 1988b). Its unusual coma morphology, combined with the possibility that different sources on the nucleus may account for outgassing during different portions of its orbit, make considerations of observing geometry important when interpreting results of ground-based composition studies and comparing across apparitions. Our observations may have sampled a dramatically different projection of the nonuniform coma into the plane of the sky than those reported in RD13. In any case, the differences in its measured volatile composition between 2003 and 2017 are pronounced.

In addition, Encke's rotation period (~11 hr; Fernández et al. 2005; Lowry & Weissman 2007; Woodney et al. 2007) is important to consider. Our longest observations of Encke on March 25 (UT 17:49–22:22) comprised ~1/3 of a complete rotation, so it is possible that active sites rotated into or out of our view during the course of both our observations and those from 2003. These (possible) rotational effects may explain the decrease in HCN in Encke from 0.17% on March 21 to 0.11% on March 25. Analysis of time series of ground-based molecular spectra obtained with IRAM and CSO of 103P/Hartley 2 found that the varying illumination of chemically heterogeneous regions on the nucleus due to rotation caused significant changes in volatile release, creating variations on timescales of hours to days (Drahus et al. 2012; Boissier et al. 2014). However, despite these strong rotational effects observed at radio wavelengths, mixing ratios of primary volatiles derived from ground-based near-infrared measurements of the bulk coma remained relatively constant (Dello Russo et al. 2011; Mumma et al. 2011).

We searched for similar short timescale variability in Encke by comparing derived HCN/H_2O in a time series of spectral extracts. Each spectral extract represented 8 minutes on-source integration time, and the entire time series spanned three hours of clock time. We found no evidence for statistically significant variation in HCN/H_2O during this time series; however, as noted earlier, this represents less than 1/3 of a complete rotation period for Encke. Thus, further measurements are needed to quantify how much (if any) impact these effects had on calculated mixing ratios during each apparition of Encke.

4.3. Comparison of Primary Volatile Mixing Ratios with Photodissociation Products

An important task in cometary science is relating measured abundances of photodissociation products (i.e., fragment species) found in optical studies to potential parent volatiles. This is a challenging endeavor, because a given fragment species can have several possible parents. In contrast, our near-infrared studies of primary volatiles suffer no such difficulty. Comparison of fragment species mixing ratios in the optical to near-infrared measurements of primary (parent) volatiles is one way to test parent−daughter relationships. In particular, we can compare the ratios C_2/OH, CN/OH, and NH/OH to our mixing ratios of C_2H_2/H_2O, HCN/H_2O, and NH_3/H_2O, respectively. Although this is an admittedly simplistic comparison, we can infer whether the mixing ratios of these primary volatiles can account for those of fragment species found in Encke. Unfortunately, the majority of the published data for Encke is taken from pre-perihelion observations. This adds an additional layer of uncertainty given its asymmetric behavior of volatile mixing ratios about perihelion observed at optical wavelengths. Additionally, with the exception of our NH_2/H_2O and NH_3/H_2O measurements, the observations of the fragment species in this comparison were not taken simultaneously with those of the primary species in this work. Thus, each of the processes mentioned in Section 4.2 may affect the comparisons; however, they are still informative.

Table 4 compares mixing ratios of primary volatiles to those of fragment species in Encke for several apparitions. The data are divided into pre- and post-perihelion observations for clarity. We note that the most direct comparisons between primary and fragment species in Encke are those reported in RD13 to published pre-perihelion fragment mixing ratios, whereas our mixing ratios are compared to post-perihelion fragment species reported in A'Hearn et al. (1985). Since A'Hearn et al. (1985) report mixing ratios over a range of R_h, we make comparisons to their measurements taken at R_h most similar to RD13 (~1.2 au) and to our measurements (~0.4 au), respectively.

For the pre-perihelion data, the mixing ratios HCN/H_2O and C_2H_2/H_2O reported in RD13 cannot account for the mixing ratios CN/OH or C_2/OH in A'Hearn et al. (1985) or any other study. This suggests that HCN and C_2H_2 are not the sole parents of CN and C_2, respectively, during the pre-perihelion portion of the 2003 apparition. Similarly, our mixing ratios HCN/H_2O and C_2H_2/H_2O cannot account for the post-perihelion mixing ratios CN/OH and C_2/OH, and so also suggest that HCN and C_2H_2 are not their sole parents. Similar trends have been observed for other short-period comets. Measured HCN/H_2O and C_2H_2/H_2O for comets 103P/Hartley 2, 6P/d'Arrest, and 45P/Honda–Mrkos–Pajdušáková cannot account for their CN/OH and C_2/OH, respectively (A'Hearn et al. 1995; Dello Russo et al. 2016a and references therein; DiSanti et al. 2017).

However, our mixing ratio NH_3/H_2O is large enough to account for both our NH_2/H_2O, as well as NH/OH reported from pre-perihelion observations, suggesting that no additional parents may be needed to explain these fragment species abundances. Our mixing ratio NH_3/H_2O is also consistent with that predicted by Dorman et al. (2013) based on their measured NH/OH.

5. Comparison to Comets as Measured at Near-Infrared Wavelengths

5.1. Comparison to Measurements of Other Comets at Small R_h

Our measurements of Encke at $R_h \sim 0.4$ au are among only a handful of IR studies of comets at $R_h < 0.8$ au. Of particular interest are OCC D/2012 S1 (ISON) and JFC 45P/

Table 4
Comparison of Primary Volatile and Fragment Species Mixing Ratios in 2P/Encke

Pre-perihelion		Post-perihelion	
Fragment Species	Primary Species	Fragment Species	Primary Species
$\log\left[\frac{Q(\mathrm{CN})}{Q(\mathrm{OH})}\right]$	$\log\left[\frac{Q(\mathrm{HCN})}{Q(\mathrm{H_2O})}\right]$	$\log\left[\frac{Q(\mathrm{CN})}{Q(\mathrm{OH})}\right]$	$\log\left[\frac{Q(\mathrm{HCN})}{Q(\mathrm{H_2O})}\right]$
−2.18[a] −2.04 ± 0.44[e]	−3.04 ± 0.11[b]	−2.54[c]	−2.91 ± 0.08[d]
$\log\left[\frac{Q(\mathrm{C_2})}{Q(\mathrm{OH})}\right]$	$\log\left[\frac{Q(\mathrm{C_2H_2})}{Q(\mathrm{H_2O})}\right]$	$\log\left[\frac{Q(\mathrm{C_2})}{Q(\mathrm{OH})}\right]$	$\log\left[\frac{Q(\mathrm{C_2H_2})}{Q(\mathrm{H_2O})}\right]$
−2.36[a] −2.23 ± 0.03[f]	<−3.09[b]	−2.76[c]	<−4.15[d]
$\log\left[\frac{Q(\mathrm{NH})}{Q(\mathrm{OH})}\right]$	$\log\left[\frac{Q(\mathrm{NH_3})}{Q(\mathrm{H_2O})}\right]$	$\log\left[\frac{Q(\mathrm{NH_2})}{Q(\mathrm{H_2O})}\right]$	$\log\left[\frac{Q(\mathrm{NH_3})}{Q(\mathrm{H_2O})}\right]$
−2.25 ± 0.03[f]	⋯	−2.62 ± 0.13[d]	−2.21 ± 0.07[d]

Notes.
[a] A'Hearn et al. (1985). Measurements acquired at $R_h = 0.9$ au during the 1984 apparition.
[b] Radeva et al. (2013). Measurements acquired at $R_h = 1.2$ au during the 2003 apparition.
[c] A'Hearn et al. (1985). Measurements acquired at $R_h = 0.62$ au during the 1984 apparition.
[d] This work.
[e] Ihalawela et al. (2011). Measurements acquired at $R_h = 1.4$ au during the 2003 apparition.
[f] Dorman et al. (2013). Measurements acquired at $R_h = 1.4$ au during the 2003 apparition.

Honda–Mrkos–Pajdušáková both of which were measured at similarly small R_h. ISON, a dynamically new, Sun-grazing OCC that was the subject of a worldwide observing campaign, showed mixing ratios of HCN, NH_3, C_2H_2, and H_2CO that increased as its heliocentric distance decreased from 0.83 au to inside 0.6 au (Dello Russo et al. 2016b; DiSanti et al. 2016). 45P/HMP, the first JFC to have its primary volatile composition sampled at $R_h < 0.8$ au, was enriched in CH_3OH, strongly depleted in CO and HCN, and consistent with respect to median values for CH_4, H_2CO, NH_3, C_2H_2, and C_2H_6 (DiSanti et al. 2017). In these respects, Encke is perhaps most similar to ISON, in that H_2CO and HCN were enriched at $R_h \sim 0.4$ au in 2017 compared to $R_h \sim 1.2$ au in 2003, however as mentioned more observations are needed to test whether this owes more to heliocentric distance rather than seasonal (pre-/post-perihelion) or other effects.

5.2. Comparison to Comet 21P/Giacobini–Zinner

JFC 21P/Giacobini–Zinner is the only other comet to have high-resolution near-infrared spectroscopic measurements spanning more than one apparition. Weaver et al. (1999) detected H_2O and CH_3OH (with mixing ratio 0.9%–1.4%), and Mumma et al. (2000) reported CO (10 ± 6%) and C_2H_6 (0.22 ± 0.13%) during the 1998 apparition. DiSanti et al. (2013) reported H_2O, CH_3OH (1.22 ± 0.11%), and C_2H_6 (0.14 ± 0.02%) from spectra obtained during its 2005 apparition. Mixing ratios of the two species measured both in 1998 and 2005 (CH_3OH and C_2H_6) were consistent in 21P/G-Z. Although these results are suggestive, the uncertainties in the 1998 measurements are relatively large, and without a more comprehensive study of its volatile inventory, it is difficult to say whether the bulk primary volatile composition of 21P/G-Z showed secular changes across apparitions. In contrast to 21P/G-Z, multiple species were compared across apparitions and with small uncertainties in Encke. Fortunately, the 2018 apparition of 21P/G-Z provides an excellent opportunity to

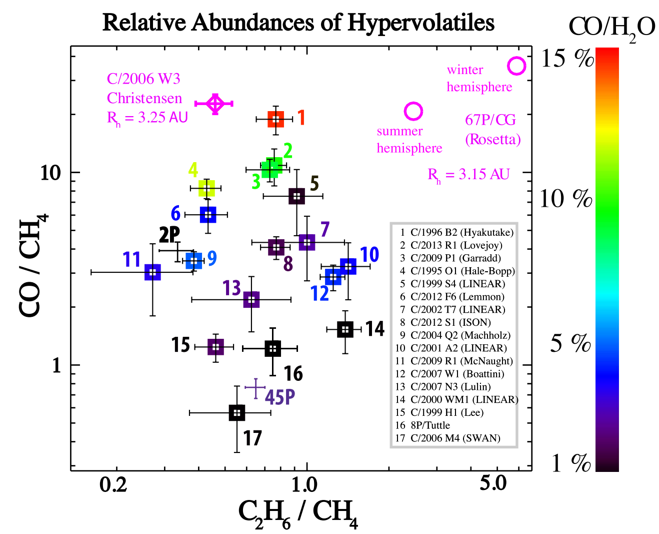

Figure 6. Ratios of hypervolatiles in comets characterized to date in the near-infrared, adapted from Bonev et al. (2017), and modified to include 2P/Encke (this work) and 45P/Honda–Mrkos–Pajdušáková (DiSanti et al. 2017). Encke is highlighted as "2P."

more completely and systematically characterize its volatile composition (see Section 6).

5.3. Hypervolatiles in Encke: CO, CH_4, and C_2H_6

CO, CH_4, and C_2H_6 (respectively) are the three most volatile molecules systematically observed in comets (Dello Russo et al. 2016a). All three hypervolatiles are depleted in Encke compared with their respective mean abundances among comets (Figure 5). Figure 6 compares our measurements ($CO/CH_4 = 3.90 \pm 0.51$ and $C_2H_6/CH_4 = 0.34 \pm 0.05$) to 18 OCCs and JFCs 67P/Churyumov–Gerasimenko (Le Roy et al. 2015) and 45P/Honda–Mrkos–Pajdušáková (DiSanti et al. 2017). For Encke the ratio CO/CH_4 falls near the median, whereas C_2H_6/CH_4 is near the low end; however,

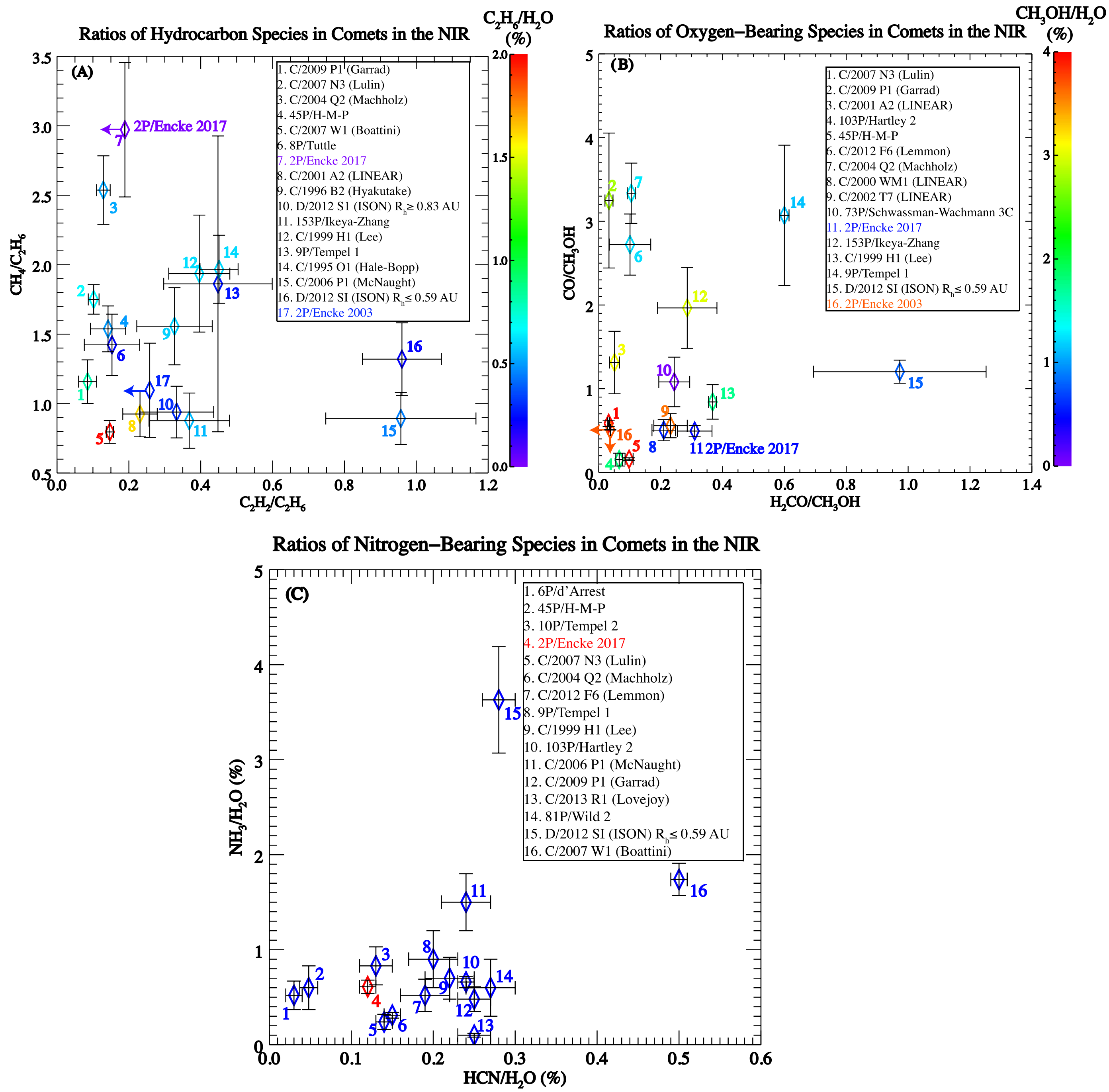

Figure 7. (A)–(C) Ratios of hydrocarbon species, oxygen-bearing species, and nitrogen-bearing species in comets as measured in the near-infrared (Dello Russo et al. 2016a; DiSanti et al. 2017). (A) Ratios of hydrocarbon species in comets. Each comet is color-coded by its ratio C_2H_6/H_2O. Encke as measured in 2017 is highlighted with a text box, and the left-facing arrow represents the 3σ upper limit C_2H_2/C_2H_6. (B) Ratios of oxygen-bearing species in comets. Each comet is color-coded by its ratio CH_3OH/H_2O. Encke in 2017 is highlighted with a text box. The 3σ upper limits H_2CO/CH_3OH and CO/CH_3OH for Encke in 2003 are represented by leftward and downward facing arrows, respectively. (C) Ratios of nitrogen-bearing species in comets. Encke is highlighted in red.

$C_2H_6/CH_4 = 0.94 \pm 0.29$ for Encke in 2003, near the median. On the other hand, 67P/CG has the highest CO/CH_4 and C_2H_6/CH_4 ratios measured in any comet, although direct comparisons between the in situ measurements of Le Roy et al. (2015) and our ground-based line of sight (bulk coma) measurements are not straightforward. Thus, it is possible that the hypervolatile content of JFCs may span the entire range of CO/CH_4 and C_2H_6/CH_4 measured among OCCs. However, with relative hypervolatile abundances characterized to date for only three ecliptic comets (compared to 18 OCCs), it is worth noting that we are still very much in the realm of *establishing* these statistics for ecliptic comets, and further observations are critically needed.

5.4. Hydrocarbon Species, Oxygen-bearing Species, and Nitrogen-bearing Species in Encke

Similarly, Encke can be compared to other comets observed at near-infrared wavelengths by examining the ratios of chemically related hydrocarbon species (CH_4, C_2H_2, C_2H_6), oxygen-bearing species (CO, H_2CO, CH_3OH), and nitrogen-bearing species (NH_3, HCN). For Encke in 2017, we found $CH_4/C_2H_6 = 2.97 \pm 0.48$ and $C_2H_2/C_2H_6 < 0.19$, $CO/CH_3OH = 0.49 \pm 0.06$ and $H_2CO/CH_3OH = 0.31 \pm 0.05$, and $NH_3/HCN = 5.08 \pm 0.72$. Figures 7(A)–(C) show these values in Encke along with corresponding measurements in comets sampled to date in the near-infrared. All values are taken from Dello Russo et al. (2016a) with the exception of 45P/Honda–Mrkos–Pajdušáková (DiSanti et al. 2017). Figure 7(A) shows that whereas Encke was closer to the median during 2003, in 2017 it was distinctly on the low end of hydrocarbon abundances among comets. Its exceptionally low mixing ratios C_2H_6/H_2O and (upper limit for) C_2H_2/H_2O are reflected in its high CH_4/C_2H_6 and low C_2H_2/C_2H_6. Figure 7(B) shows that in 2017 Encke was near the median in its oxygen-bearing species content (relative to CH_3OH), yet in 2003 it was among the lowest values in measured comets, owing largely to its enriched CH_3OH. This change in oxygen-bearing species abundances can be attributed to the significant differences in H_2CO/H_2O and CH_3OH/H_2O between 2003 and 2017 measurements. Figure 7(C) shows that Encke is among depleted comets in nitrogen-bearing species.

5.5. *Encke in the Context of the Comet Population*

As in RD13, the 2017 apparition of Encke showed a comet that does not easily fit into any existing taxonomic classification. Although no species were found to be enriched in 2017 compared to mean values among comets, two species (H_2CO and NH_3) were similar to the mean, and all others were depleted to varying degrees. Dello Russo et al. (2016a) proposed a classification system based on primary volatile abundances using cluster analysis. Based on its composition as measured in 2003, Encke falls within Group B (hydrocarbon, HCN, H_2CO, and CO poor-to-typical), and is most similar to Subgroup 4 (hydrocarbon, HCN, and H_2CO poor, CH_3OH typical). However, Encke does not fall into the same Group (or Subgroup) based on our 2017 study reported here. Rather, Encke belongs within Group A (hydrocarbon, CH_3OH, and CO poor) and is most similar to Subgroup 2 (hydrocarbon, CH_3OH, and CO poor, H_2CO and HCN typical).

Encke's place within these groupings during each apparition is not surprising. Ecliptic comets (JFCs and Encke-type) are most likely to be found in Groups A and B, reflecting the generally depleted nature of their volatile content. However, one could reasonably expect to have found Encke in Group C based on its composition as measured in 2017. This group is mostly populated by comets that were observed at small R_h such as Encke (0.45–0.53 au) or after a perihelion passage well within 1 au. This is perhaps reflective of the nature of volatile release at small R_h, which can originate from native ices and/or from thermal degradation of grains (Dello Russo et al. 2016a). Perhaps Encke is an exception to this trend due to its status as the most thermally evolved comet known, as evidenced by its strongly depleted volatile content. Clearly, more work is needed to further improve the evolving taxonomy based on primary volatile composition.

6. Summary of Results for 2P/Encke and Upcoming Opportunities

We detected fluorescent emission from a suite of primary volatiles (H_2O, CO, C_2H_6, CH_3OH, CH_4, H_2CO, NH_3, OCS, and HCN) and three fragment species (OH^*, NH_2, and CN) in ecliptic comet 2P/Encke, and stringently constrained the primary volatile C_2H_2, using the recently commissioned iSHELL spectrograph at the NASA IRTF. The highly favorable 2017 apparition of Encke featured sufficient geocentric velocity to permit secure detections of the hypervolatiles CO and CH_4, further laying the groundwork for establishing robust statistics for these species in ecliptic comets. The excellent sensitivity, large spectral grasp, and unique daytime guiding capabilities of iSHELL allowed us to provide the first comprehensive comparison of primary volatile composition in a comet across multiple apparitions. We found dramatic differences in the mixing ratios of several primary volatiles in 2017 compared to those reported from 2003. We discussed possible mechanisms for these effects, including the possibility of distinct, chemically heterogeneous sources in the nucleus, additional sources (e.g., dust) at small heliocentric distances, and pre-/post-perihelion asymmetries in volatile release.

Ground-based studies of primary volatile composition of comets are critical to interpreting the (continually evolving) taxonomy of comets and relating measured mixing ratios to conditions in the proto-solar nebula where and when a given comet formed. It is yet another reminder of the extensive compositional diversity among comets in that one short-period ecliptic comet (Encke) showed clear differences in coma composition across apparitions, whereas another (21P/Giacobini–Zinner) may not (Section 5.2). This reinforces the difficulty of drawing conclusions from a single body based on limited observations during a given apparition. Fortunately, the 2018 apparition of 21P/G-Z is favorable, and an extensive campaign (including both pre- and post-perihelion observations) is planned. Additionally, the bright comet 46P/Wirtanen will make a historic apparition in 2018 December, passing within 30 lunar distances of Earth near perihelion. A global, multi-wavelength observing campaign is planned, which will reveal the composition and spatial distributions of volatiles in the coma of 46P/Wirtanen at more nearly mission-scale sensitivities. These observations may shed further light on potential differences in composition, both about perihelion and across apparitions, for ecliptic comets.

Further studies that address each of these pressing areas in cometary science (i.e., observations at small R_h, pre-/post-perihelion, and comparisons across multiple apparitions) are needed to answer questions stimulated by our 2017 study of the peculiar comet 2P/Encke. We anticipate that iSHELL and its state-of-the-art observing capabilities will play an important role in making these studies possible, and in furthering our knowledge of the volatile content of comets and the early solar system.

Data for this study were obtained at the NASA Infrared Telescope Facility (IRTF), operated by the University of Hawai'i under contract NNH14CK55B with the National Aeronautics and Space Administration. We are most fortunate to have the opportunity to conduct observations from Maunakea, and recognize and acknowledge the very significant cultural role and reverence that the summit of Maunakea has always had within the indigenous Hawaiian community. This study was generously funded by NASA Planetary Astronomy/Solar System Observations (NNX12AG24G, 15-SSO15_2-0028, 80NSSC17K0705) and Planetary Atmospheres/Solar System Workings Programs (NNX12AG60G, NNX17AC86G), the NASA Astrobiology Institute (13-13NAI7_2_0032), the National Science Foundation (AST-1616306, AST-1615441), and NASA Headquarters under the NASA Earth and Space Science Fellowship Program (Grant NNX16AP49H), and

International Space Science Institute Team 361. We thank an anonymous reviewer for suggestions that improved the paper. We acknowledge and thank the entire staff at IRTF, particularly B. Bus, G. Osterman, and T. Matulonis for their assistance and professionalism in carrying out our challenging observations of 2P/Encke, which took place entirely during daytime and at a solar elongation of only 25°.

ORCID iDs

Nathan X. Roth https://orcid.org/0000-0002-6006-9574
Erika L. Gibb https://orcid.org/0000-0003-0142-5265
Boncho P. Bonev https://orcid.org/0000-0002-6391-4817
Michael A. DiSanti https://orcid.org/0000-0001-8843-7511
Neil Dello Russo https://orcid.org/0000-0002-8379-7304
Ronald J. Vervack, Jr. https://orcid.org/0000-0002-8227-9564
Adam J. McKay https://orcid.org/0000-0002-0622-2400
Hideyo Kawakita https://orcid.org/0000-0003-2011-9159

References

A'Hearn, M. F., Belton, M. J. S., Delamere, W. A., et al. 2011, Sci, 332, 1396
A'Hearn, M. F., Birch, P. V., Feldman, P. D., & Millis, R. L. 1985, Icar, 64, 1
A'Hearn, M. F., Millis, R. L., Schleicher, D. G., Osip, D. J., & Birch, V. P. 1995, Icar, 118, 223
Bockelée-Morvan, D., Crovisier, J., Erard, S., et al. 2016, MNRAS, 462, S170
Bodewits, D., Farnham, T. L., A'Hearn, M. F., et al. 2014, ApJ, 786, 48
Boissier, J., Bockelée-Morvan, D., Biver, N., et al. 2014, Icar, 228, 197
Bonev, B. P. 2005, PhD thesis, Univ. Toledo
Bonev, B. P., & Mumma, M. J. 2006, ApJ, 653, 788
Bonev, B. P., Mumma, M. J., DiSanti, M. A., et al. 2006, ApJ, 653, 774
Bonev, B. P., Mumma, M. J., Radeva, Y. L., et al. 2008, ApJL, 680, L61
Bonev, B. P., Mumma, M. J., Villanueva, G. L., et al. 2007, ApJL, 661, L97
Bonev, B. P., Villanueva, G. L., DiSanti, M. A., et al. 2017, AJ, 153, 241
Bregman, J. D., Witteborn, F. C., Allamandola, L. J., et al. 1987, A&A, 187, 616
Brooke, T. Y., Weaver, H. A., Chin, G., et al. 2003, Icar, 166, 167
Cordiner, M. A., Remijan, A. J., Boissier, J., et al. 2014, ApJL, 792, L2
Crovisier, J., Biver, N., Bockelée-Morvan, D., & Colom, P. 2009, P&SS, 57, 1162
Crovisier, J., Brooke, T. Y., Hanner, M. S., et al. 1996, A&A, 315, L385
Dello Russo, N., DiSanti, M. A., Magee-Sauer, K., et al. 2004, Icar, 168, 186
Dello Russo, N., DiSanti, M. A., Mumma, M. J., Magee-Sauer, K., & Rettig, T. W. 1998, Icar, 135, 377
Dello Russo, N., Kawakita, H., Vervack, R. J., Jr., & Weaver, H. A. 2016a, Icar, 278, 301
Dello Russo, N., Vervack, R. J., Jr., Kawakita, H., et al. 2016b, Icar, 266, 152
Dello Russo, N., Vervack, R. J., Jr., Lisse, C. M., et al. 2011, ApJL, 734, L8
DiSanti, M. A., Bonev, B. P., Dello Russo, N., et al. 2017, AJ, 154, 246
DiSanti, M. A., Bonev, B. P., Gibb, E. L., et al. 2016, ApJ, 820, 34
DiSanti, M. A., Bonev, B. P., Magee-Sauer, K., et al. 2006, ApJ, 650, 470
DiSanti, M. A., Bonev, B. P., Villanueva, G. L., et al. 2013, ApJ, 763, 1
DiSanti, M. A., Mumma, M. J., Dello Russo, N., et al. 2003, JGRE, 108, 5061
DiSanti, M. A., Mumma, M. J., Dello Russo, N., & Magee-Sauer, K. 2001, Icar, 153, 361
DiSanti, M. A., Villanueva, G. L., Paganini, L., et al. 2014, Icar, 228, 167
Dorman, G., Pierce, D. M., & Cochran, A. L. 2013, ApJ, 778, 140
Drahus, M., Jewitt, D., Guilbert-Lepoutre, A., Waniak, W., & Sievers, A. 2012, ApJ, 756, 80
Farnham, T. L. 2009, P&SS, 57, 1192
Feaga, L. M., A'Hearn, M. F., Farnham, T. L., et al. 2014, AJ, 147, 24
Fernández, Y. R., Lowry, S. C., Weissman, P. R., et al. 2005, Icar, 175, 194
Ferrin, I. 2008, Icar, 197, 169
Fink, U., Doose, L., Rinaldi, G., et al. 2016, Icar, 277, 78
Fray, N., Bénilan, Y., Biver, N., et al. 2006, Icar, 184, 239
Gibb, E. L., Bonev, B. P., Villanueva, G. L., et al. 2012, ApJ, 750, 102
Gibb, E. L., Mumma, M. J., Dello Russo, N., et al. 2003, Icar, 165, 391
Gomes, R., Levison, H. F., Tsiganis, K., & Morbidelli, A. 2005, Natur, 435, 466
Harker, D. E., Woodward, C. E., & Wooden, D. H. 2005, Sci, 310, 278
Hässig, M., Altwegg, K., Balsiger, H., et al. 2015, Sci, 347, aaa0276
Ihalawela, C. A., Pierce, D. M., Dorman, G. R., & Cochran, A. L. 2011, ApJ, 741, 89
Kawakita, H., Dello Russo, N., Vervack, R. J., Jr., et al. 2014, ApJ, 788, 110
Le Roy, L., Altwegg, K., Balsiger, H., et al. 2015, A&A, 583, A1
Levison, H. F., Morbidelli, A., Tsiganis, K., et al. 2011, AJ, 142, 152
Levison, H. F., Terrel, D., Wieger, P. A., et al. 2006, Icar, 182, 161
Lowry, S. C., & Weissman, P. R. 2007, Icar, 188, 212
Luspay-Kuti, A., Hässig, M., Fuselier, S. A., et al. 2015, A&A, 583, A4
Magee-Sauer, K., Mumma, M. J., DiSanti, M. A., et al. 1999, Icar, 142, 498
McKay, A. J., Cochran, A. L., DiSanti, M. A., et al. 2015, Icar, 250, 504
Morbidelli, A., Levison, H. F., Tisganis, K., & Gomes, R. 2005, Natur, 435, 462
Mumma, M. J., Bonev, B. P., Villanueva, G. L., et al. 2011, ApJL, 734, L7
Mumma, M. J., DiSanti, M. A., Dello Russo, N., et al. 2000, ApJL, 531, L155
Mumma, M. J., McLean, I. S., DiSanti, M. A., et al. 2001, ApJ, 546, 1183
Paganini, L., DiSanti, M. A., Mumma, M. J., et al. 2014, AJ, 147, 15
Paganini, L., Mumma, M. J., Villanueva, G. L., et al. 2012, ApJL, 748, L13
Protopapa, S., Sunshine, J. M., Feaga, L. M., et al. 2014, Icar, 238, 191
Radeva, Y. L., Mumma, M. J., Bonev, B. P., et al. 2010, Icar, 206, 764
Radeva, Y. L., Mumma, M. J., Villanueva, G. L., et al. 2013, Icar, 223, 298
Rayner, J., Bond, T., Bonnet, M., et al. 2012, Proc. SPIE, 8446, 84462C
Rayner, J., Tokunaga, A., Jaffe, D., et al. 2016, Proc. SPIE, 9908, 990884
Rickman, H., Marchi, S., A'Hearn, M. F., et al. 2015, A&A, 583, A44
Sekanina, Z. 1988a, AJ, 95, 911
Sekanina, Z. 1988b, AJ, 96, 1455
Stern, S. A. 2003, Natur, 424, 639
Villanueva, G. L., Mumma, M. J., Bonev, B. P., et al. 2009, ApJL, 690, L5
Villanueva, G. L., Mumma, M. J., DiSanti, M. A., et al. 2011, Icar, 216, 227
Villanueva, G. L., Mumma, M. J., Novak, R. E., & Hewagama, T. 2008, Icar, 195, 34
Weaver, H. A., Chin, G., Bockelée-Morvan, D., et al. 1999, Icar, 142, 482
Wooden, D. H., Woodward, C. E., & Harker, D. E. 2004, ApJL, 612, L77
Woodney, L. M., Schleicher, D. G., Reetz, K. M., & Ryan, K. J. 2007, AAS/DPS Meeting, 38, 486
Xie, X., & Mumma, M. J. 1996a, ApJ, 464, 442
Xie, X., & Mumma, M. J. 1996b, ApJ, 464, 457
Zolensky, M. E., Zega, T. J., Yano, H., et al. 2006, Sci, 314, 1735